Thesis Title

A subtitle of your thesis

Author name

Thesis submitted for the degree of
Master in Master's Program Name <change at main.tex>
60 credits

Department Name <change at main.tex>
Faculty name <change in duoforside.tex>

UNIVERSITY OF OSLO

Spring 2022

Thesis Title

A subtitle of your thesis

Author name

© 2022 Author name

Thesis Title

http://www.duo.uio.no/

Printed: Reprosentralen, University of Oslo

Abstract

Contents

1 Introduction **1**

I Theory **3**

2 High-Entropy alloys **4**
- 2.1 Fundamentals 4
- 2.2 Core effects and properties 7

3 Modeling of random alloys **9**
- 3.1 The Special Quasi-random Structure model 9
  - 3.1.1 Mathematical description 10
  - 3.1.2 Applications to high-entropy alloys 12

4 Density Functional Theory **16**
- 4.1 Review of Quantum Mechanics 17
  - 4.1.1 The Shrodinger equation 17
  - 4.1.2 Approximations to the many-body Shrodinger equation 18
- 4.2 Kohn-Sham density functional theory 20
  - 4.2.1 Density functional theory 20
  - 4.2.2 The Kohn-Sham Equation 21
- 4.3 Limitations of DFT - Insert refs 22

II Methodology and Implementation **24**

5 Practical application of DFT **25**
- 5.1 The Exchange-Correlation functional 25
  - 5.1.1 Local density approximation 25
  - 5.1.2 Generalized gradient approximation 26
  - 5.1.3 Meta-GGA 26
  - 5.1.4 Hybrid functionals 27
  - 5.1.5 Outlook 27
- 5.2 Fundamental aspects of practical DFT calculations 28
- 5.3 Self-consistent field calculation 30

6 Computational details **32**
6.1 Vienna Ab initio Simulation Package 32
6.2 Generation of SQS 34
6.3 Utility scripts 35

III Results and Discussion **37**

7 The results of equimolar (CrFeMnNi)Si_2 in the $\beta-$FeSi$_2$ structure **39**
7.1 The band gap 41
7.2 Local and projected density of states 44
7.3 Results from SCAN and HSE06 functionals 46
7.4 Pair distribution functions 51
7.5 SQS size 53

8 Permutations of (CrFeMnNi)Si_2 **58**

9 Different compositions and crystal structure **63**
9.1 New compositions 63

10 Overview and outlook **65**
10.1 Literature 65
10.2 General thoughts 66
10.3 Other things 70
10.4 $Cr_4Fe_4Mn_4Ni_4Si_{32}$ in different crystal structures 73
10.5 Overview 75

IV Conclusion **76**

A Compositions **73**
A.1 Projected density of states 73
A.2 Probability distribution functions 76

B Eqvimolar alloy **78**
B.1 DOS 78

C Charge density **80**

List of Figures

2.1 Formation of HEA based on δ and N. Figures adopted from [**hea2016_ch2**] 6
2.2 A schematic illustration of lattice distortion in high-entropy alloys. Figure from [**owen_jones_2018**] 8

3.1 PDFs of (a) 20 and (b) 250 atom SQS models of CrFeMnNi [**hea2016_ch10**] 13
3.2 Density of states with SQS and MC/MD of FCC CoCrFeNi, figure from [**hea2016_ch10**] 14
3.3 Probability distribution functions with SQS and MC/MD of HCP CoOsReRu [**hea2016_ch10**] 14

4.1 Number of DFT studies per year from 1980 to 2021 [**dimensions**]. 16

5.1 Calculated to experimental band gap measurements of Becke-Johnsoon, modified Becke-Johnson and SCAN functionals [**xc_benchmark**] 27
5.2 Self consistent iteration of a DFT calculation. Figure adopted from lecture notes fys-mena4111 **cite** 31

6.1 48 atom SQS based on eqvimolar distribution of Cr, Fe, Mn and Ni in and $FeSi_2$ cell. 36

7.1 Density of states of SQS D (CrFeMnNi)Si_2 with PBE. 41
7.2 Density of states of SQS B (CrFeMnNi)Si_2 with PBE. 41
7.3 Local density of states of Si (SQS D) 44
7.4 Local density of states of (a) Cr, (b) Mn, (c) Fe, (d) Ni in SQS D. 44
7.5 Projected density of states SQS D CFMN (fesi2) from PBE calculation 45
7.6 Projected density of states of SQS D and B around E_F 45
7.7 Density of states illustrating the band gaps from PBE and SCAN calculations for SQS E and D. 47
7.8 Density of states of SQS B with HSE06 47
7.9 Probability distribution function of SQS D (top) and B (bottom) 51
7.10 CPU time, **Make log plot instead** 53
7.11 Density of states of SQS E 192 atom SQS. 55
7.12 Pair distribution functions of SQS sizes (top) 48 atoms, (middle) 96 atoms, (bottom) 192 atoms 56

8.1 Projected density of states of (a) $Cr_3Fe_3Mn_7Ni_3Si_{32}$ (SQS B), (b) $Cr_5Fe_5Mn_3Ni_3Si_{32}$ (SQS C), (c) $Cr_5Fe_3Mn_5Ni_3Si_{32}$ (SQS A), (d) $Cr_3Fe_5Mn_5Ni_3Si_{32}$ (SQS D) 61
8.2 Projected density of states of $Cr_3Fe_3Mn_3Ni_7Si_{32}$ around E_F . 62

9.1 Projected density of states of (CrFeMnCo)Si_2. 65
9.2 Density of states of a) (CrFeCoNi)Si_2 and b) (CrFeTiNi)Si_2. . 66
9.3 Density of states of two SQSs of (CoFeMnNi)Si_2. 66

A.1 chCr4Fe4Co4Ni4Si32 73
A.2 chCo4Fe4Mn4Ni4Si32 74
A.3 chCr4Fe4Mn4Co4Si32 74
A.4 chCr4Fe4Ti4Ni4Si32 75
A.5 chCr4Fe4Mn4Ti4Si32 75
A.6 Probability distribution functions of top: $Co_4Fe_4Mn_4Ni_4Si_{32}$ (SQS D), middle: $Cr_4Fe_4Co_4Ni_4Si_{32}$ (SQS B), bottom: $Cr_4Fe_4Mn_4Co_4Si_{32}$ (SQS B) 76
A.7 Probability distribution function of top: $Cr_4Fe_4Mn_4Ti_4Si_{32}$ (SQS B), bottom: $Cr_4Fe_4Ti_4Ni_4Si_{32}$ (SQS B)) 77

B.1 Density of states SQS A (CrFeMnNi)Si_2 with PBE. 78
B.2 Density of states SQS E (CrFeMnNi)Si_2 with PBE. 79

List of Tables

7.1 Total energy per atom, final magnetic moment and band gap of 5 unique SQS of (CrFeMnNi)Si_2 based on the $\beta-$ $FeSi_2$ unit cell. 40
7.2 Band gap of the 5 SQSs of (CrFeMnNi)Si_2 calculated from the eigenvalues in spin up, down and total. 42
7.3 Band gap of SQS D as a function of occupancy in the eigenvalues. 43
7.4 Band gap calculated with PBE, SCAN and HSE06 XC-functionals of (CrFeMnNi)Si_2 SQSs. 46
7.5 Minimum gap between k-point in valence band and conduction band in SQS B from PBE, SCAN and HSE06 48
7.6 Band gap from HSE06 calculations with gaussian smearing and smearing width *sigma* equal to 0.05 and 0.005, and the tetrahedron method (TBC). "-" mean unchanged values, "ND" means not done. 49
7.7 Overivew 48, 96 and 192 SQSs. 53
7.8 Band gap of SQSs of 48, 96 and 192 atoms each of (CrFeMnNi)Si_2. The names are arbitrary, ie A in 48 does not equal A in 96 or 192. 54

8.1 Summary composition diagram 58
8.2 Band gaps of various compositions of (CrFeMnNi)Si_2. Most stable SQS of a set is highlighted in bold text, defect band gap are listed in cursive. Some SQSs were excluded from the table due to unsuccessful calculations. 60

9.1 Overview new compositions 63
9.2 Final magnetic moment of the most stable supercell of each composition. 64
9.3 Band gaps of the most stable SQS of $\beta-$ $FeSi_2$ high-entropy silicide compositions as a function of occupancy in the eigenvalues. 65

10.1 Mean and stadard deviation of the total energy and magnetic moment per atom, plus enthalpy of formation of the listed mean energies ($FeSi_2$). 68

10.2 Total and spin dependent band gap of 4 permutations of CFMN (fesi2) with PBE GGA calculation. The structures that are excluded from this list either failed in calculations, or does not show any band gap.< 70

Preface

Chapter 1

Introduction

some introduction on the importance of discovering new materials and alloying.
Need something on thermoelectricity related to both the band gap and high-entropy alloys.

High-entropy alloys is a novel class of materials based on alloying multiple components, as opposed to the more traditional binary alloys. This results in an unprecedented opportunity for discovery of new materials with a superior degree of tuning for specific properties and applications. Recent research on high-entropy alloys have resulted in materials with exceedingly strong mechanical properties such as strength, corrosion and temperature resistance, etc **find references**. Meanwhile, the functional properties of high-entropy alloys is vastly unexplored. In this study, we attempt to broaden the knowledge of this field, the precise formulation of this thesis would be an exploration on the possibilities of semiconducting high-entropy alloys.

A key motivation of this thesis is the ability to perform such a broad study of complex materials in light of the advances in material informatics and computational methods. In this project, we will employ Ab initio methods backed by density functional theory on top-of the line supercomputers and software. 20 years ago, at the breaking point of these methods, this study would have been significantly narrower and less detailed firstly, but secondly would have totaled ... amount of CPU hours to complete (**Calculate this number**). In the addition to the development in computational power, is also the progress of modeling materials, specifically we will apply a method called Special Quasi-random Structures (SQS) to model high-entropy alloys or generally computationally complex structures. Together with the open landscape of high-entropy alloys described above, these factors produce a relevant study in the direction of applying modern computational methods to progress the research of a novel material class and point to promising directions for future research.

In specifics, this thesis revolve around the electrical properties of high-entropy alloys, mainly the band gap as this is the key indicator for a semiconducting material and it's applicability. Semiconductors are the building blocks in many different applications in today's world, ranging from optical and electrical devices, to renewable energy sources such as solar and thermoelectricity. Given the economic and sustainable factors concerning silicon, in addition to its role in relevant applications such as microelectronics and solar power. Silicon emerges as a natural selection to build our alloys around. Furthermore, the development and research on both high entropy alloys and metal silcides have been heavily centered around 3d transition metals. Keeping in line with the economic and environmental factors, we will continue this direction by focusing on high entropy stabilized sustainable and economic 3d metal silicides **Not happy with this writing**. Throughout the study we will analyze a great number of permutations of 3d silicides, from different initial metal silicides such as $CrSi_2, FeSi_2, MnSi_{1.75}, Fe_2Si$, each with distinct properties relating to the band gap, crystal structure and metal to silicon ratio. In addition, the permutations include numerous metal distributions and elements within the 3d-group of metals. Examples are Co, Cr, Fe, Mn, and Ni.

Given a background in high-entropy alloys, one could ask if this study is truly sensible. In the later sections we will cover the details of this field, and it quickly become clear that the materials investigated in this study does not fall under the precise definition of high-entropy alloys, nor do we intend to explore the properties and factors relating to high-entropy stabilized alloys such as the configurational entropy, phase stability and finite temperature studies. However this study is motivated from the discovery of these materials and promising properties, and venture into a more hypothetical space of materials, enabled by the computational methods available to study the potential properties of such materials. On the other hand, very recent studies **Mari, and other HEA silicide study** have experimentally synthesized high-entropy disilicides, thus in some way justifying the direction of this project.

We begin this project by reviewing key concepts of solid-state physics for readers lacking a background in materials science, and an introduction to the base 3d silicides of the experimental work. Later follows a theoretic walk-through of the relevant concepts of this thesis, these topics include high-entropy alloys, special quasi-random structures, and density functional theory. Next we shine light on the implementation of DFT in this project, and other computational details required to reproduce the results in this thesis, such as the use of the Vienna Ab Initio Simulation Package (VASP) and implementation of SQS. Finally we present the results of our study, these include the band gap and electronic properties of various structures and the success and challenges of the computational methods applied throughout the study.

Part I

Theory

Part II

Methodology and Implementation

Part III

Results and Discussion

Change this introduction to fit the final product! In this one year long project, we have collected results of a great number of materials with various structures and compositions. The initial experimentation was based on high-entropy silicides of the Fe_2Si unit cell, created from the special quasi-random structure approach as described above. Despite the non-semiconducting character of this compound, we worked under the idea that the extraordinary properties that have been observed in high-entropy alloys through effects such as the cocktail effect, we could discover specific combinations of elements that would yield a semiconductor. In addition, the ratio between silicon atoms to metals allowed us to create nearly eqvimolar high-entropy alloys.

Following this attempt, we transitioned into studying high-entropy silicides based on well known semiconducting 3d silicides such as $\beta-FeSi_2$, $CrSi_2$ and $MnSi_{1.75}$. The main outcome of this project is that for all 4 different starting silicides, we could only produce high-entropy silicides from one unit cell, furthermore in this cell only one specific compositions of elements was semiconducting. This was $Cr_{0.25}Fe_{0\cdot 25}Mn_{0.25}Ni_{0.25})Si_2$, herein CFMN, in the $\beta-$ $FeSi_2$ crystal structure.

This section will be structured in the following manner, firstly we will investigate the CFMN (fesi2) compound and various permutations of the composition. Thereafter we will look at other possible compositions of fesi2 based high-entropy silicides, and lastly test the CFMN composition in other crystal symmetries. In final we will present an overview of the complete study and the various compounds that have been investigated in order to propose promising directions and guideline future research directions in this field. In this way, we aim to understand the uniqe properties of CFMN (fesi2) and why this particular compound is semiconducting compared to the other testes structures in this project. Properties we will cover is the overall stability by total energy and corresponding enthalpy of formation, the magnetic properties and which elements contribute to the magnetism. But in majority, we will look at the band gap and related properties, as this is the main motivation and distinction of the study.

Add figure DOS FeSi2?

Chapter 7

The results of equimolar (CrFeMnNi)Si_2 in the $\beta-$FeSi$_2$ structure

$\beta - FeSi_2$ in the orthorombic cmce crystal lattice is a well known semiconductor with an experimentally measured band gap of around 0.85 ev at room temperature [1], the nature of the band gap is under debate, all though most ab inito studies point to an indirect gap, experimental work indicate a direct gap. From our calculations we find an indirect band gap close to 0.65 eV with PBE, compared for example materials project's listed value of 0.698 eV with the same functional. Moreover in agreement with the calculations of materials project we discover that bulk $\beta-$ FeSi$_2$ is diamagnetic. Finally, the enthalpy of formation of this compound is calculated as $-18.6583eV$.

The high-entropy alloys generated from the FeSi$_2$ unit cell alloys can be seen in figure 6.1. The supercells consist of 48 atoms each, in which the 16 iron sites is occupied equimolarly between Cr, Fe, Mn, and Ni, and the 32 silicon sites is as before occupied by silicon. Bellow in table 7.1 we list the total energy per atom (Toten), final magnetic moment (Mag) and band gap (E_G) of the five distinct SQSs, plus the mean and standard deviation (std) of the set, and enthalpy of formation ΔH of the mean energy. For simplicity we denote the 5 supercells as A, B, C, D and E.

SQS	Toten (eV)	Mag (μ_B)	E_G (eV)
A	-6,6080	0.0833	0.0280
B	-6,6138	0.0833	0.0523
C	-6,6063	0.0834	0.0344
D	-6,6155	0.0833	0
E	-6,6089	0.0833	0.0495
Mean	-6.6105	0.0833	0.0328
Std	0.0039	0.0000	0.0210
ΔH	-11.5000 eV	-	-

Table 7.1: Total energy per atom, final magnetic moment and band gap of 5 unique SQS of (CrFeMnNi)Si_2 based on the $\beta-$ $FeSi_2$ unit cell.

From a first glance it's a clear distinction between the SQSs, especially in terms of the band gap and less so for the total magnetic moment. On the grounds of the total energy we note that the most stable supercell is SQS D, and reversely the least stable is SQS A. The band gaps listed in table 7.1 point to that the large majority of the SQSs are narrow-gap semiconductors in the range 0.028 - 0.052 eV, but the utmost stable configuration D does not exhibit any finite band gap.

In terms of the magnetism we see that contrary to the bulk $FeSi_2$ compound that this alloy is magnetic. Investigating the local magnetic moments of SQS D we discover that the ferromagnetic iron and nickel contain very small moments and non-existent in Ni.On the other hand the anti-ferromagnetic elements chromium and manganese contain large magnetic moments. In section 2.2 we provided several examples where Cr was known to reduce the saturation magnetization of high-entropy alloys. For example in the ferromagnetic HEA CoFeMnNiX, X = Al, Cr, Ga, Sn, studied in [2]. Mn had minimal impact on the magnetism and favoured the ferromagnetic phase, meanwhile addition of Cr pushed the material to a paramagnetic phase. Likewise in the eqvimolar system of CrMnFeCoNi [3], the local magnetic moment of Cr was found to align antiferromagnetic, and the ferromagnetic character was attributed to local magnetic moments of Fe and Mn. The odd magnetic properties experienced in this alloy can be related to several factors. Firstly are the limitations mentioned previously about about both DFT and special quasi-random structures to model magnetic and particularly paramagnetic materials. Further the magnetic investigation and focus in this project have been very superficial with only considering non-spin polarized calculations or co-linear spin polarization, thus the phases in-between have been neglected. Lastly only the the ground state, ie 0K have been studied. Hence the reported magnetic properties should be taken with a grain of salt and are intended for subsequent studies focused on the magnetic properties of this alloy especially at non-zero temperatures.

7.1 The band gap

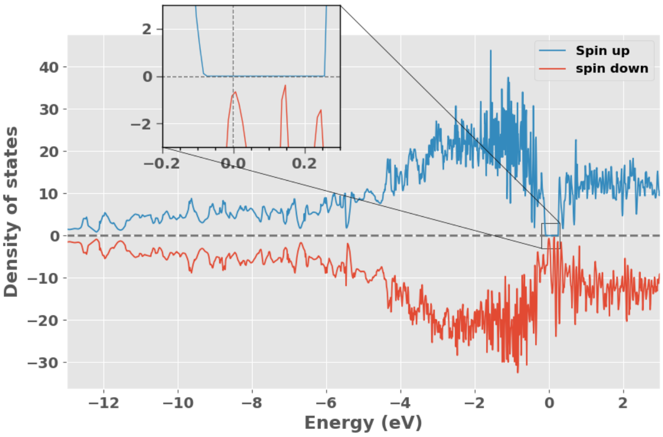

Figure 7.1: Density of states of SQS D (CrFeMnNi)Si_2 with PBE.

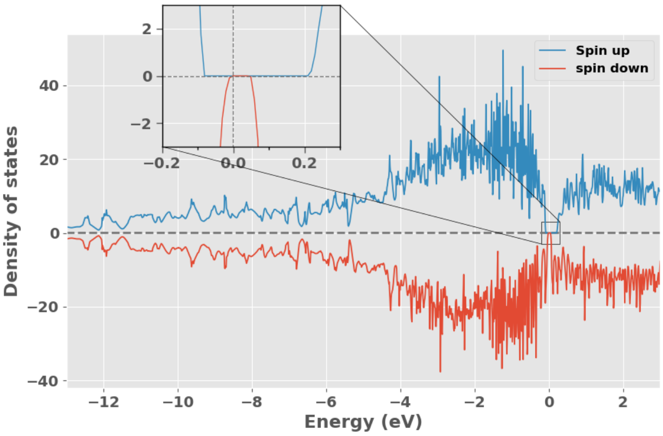

Figure 7.2: Density of states of SQS B (CrFeMnNi)Si_2 with PBE.

Above we plot the electronic density of states of SQS D and B from calculations with the PBE GGA functional. These supercells and corresponding properties are emphasized due to the relative stability in the set. Being the most stable means it's the most representative structure of the potentially "real" material, and hence so are the properties of that SQS. From the DOS in figure 7.1 we discover that the structure is in fact a half-metal with a band gap around 0.3 eV in the spin up channel and a metal in spin down. The exact value of the band gap in spin up is calculated from the range of energies corresponding 0 density of states around E_F, ie $0.2eV - (-0.1eV) = 0.3eV$. Following the total band gap of the solid is determined by the minimum range of energies from both spins, which in this case is 0 from the spin down DOS. Since these values are calculated by the density of states they will be denoted as $E_G^{\text{up, dos}}$ and $E_G^{\text{dw, dos}}$ to indicate the spin direction. By the same mannerism we can see from figure 7.2 that the second utmost stable SQS (B) clearly contain finite values of both $E_G^{\text{up, dos}}$ and $E_G^{\text{dw, dos}}$. Similar figures can be seen for SQS A, C, and E in appendix .., all respective spin dependent band gaps is listed below in table 7.2.

These values are determined from the calculated eigenvalues, and hence will be referenced to as $E_G^{\text{up, eigen}}$ and $E_G^{\text{dw, eigen}}$. This value is found by subtracting the highest energy eigenvalue in the valence band from the lowest energy eigenvalue in the conduction band. Across all five SQSs we observe in accordance with the magnetic property a distinction between spins where $E_G^{\text{up}} > E_G^{\text{dw}}$.

SQS	$E_G^{\text{up, eigen}}$ (meV)	$E_G^{\text{dw, eigen}}$ (meV)	$E_G^{\text{tot, eigen}}$ (meV)
A	81.4	52.2	28.1
B	293	52.2	52.2
C	236	34.3	34.3
D	339	0.00	0.00
E	308	50.0	50.0

Table 7.2: Band gap of the 5 SQSs of (CrFeMnNi)Si$_2$ calculated from the eigenvalues in spin up, down and total.

Alike the bulk material, these gaps are indirect. It would have been instructive to visualize and analyze the energy bands by plotting the band structure. Unfortunately this is neither simple to perform or interpret in large supercells consisting of several elements and a large number of energy bands. One solution is to do band-unfolding, but given the complex structure and implementation of the special quasi-random structures method in VASP this proved too challenging for the scope of this project.

A key point regarding the band structure of SQS D is the presence of defect states. In this structure the highest occupied conduction band is 128 for spin up states and band 124 in spin down, thus a difference of 4 bands between spins. For the spin down states we find that the highest energy conduction band, ie 124 have states with occupancy both slightly bellow 1.00 and above at several k-points. Likewise the lowest energy valence band (124) have partially filled states above 0.00 and bellow. The case of occupancy either above or bellow completely full or completely empty is simply a numerical inaccuracy well-known to calculations that apply the Tetrahedron method with Bloch corrections and have no real impact on the results. The second case where we have partially filled eigenstates in the conduction band and not completely filled states is a familiar term in random alloys [4] in which the forbidden energy gap is contaminated by defect states. To further study this effect we introduce $E_G^{\text{eigen}}(occ)$ to represent the band gap calculated at a cut-off occupancy in the eigenvalues such that $E_G^{\text{eigen}}(0.99)$ only consider eigenstates with occupancy above 0.99 as filled. Equivalently $E_G^{\text{eigen}}(0.01)$ only consider eigenstates with occupancy less than 0.01 as empty. In the following results we will list the occupancy parameter as a single value, such that $occ = 0.1$ represent occupancy equal to 1- 0.1 and 0 + 0.1. Applying this to SQS D we get the results listed below in table .., keep in mind that $E_G^{\text{up, eigen}}$ is constant from that the defect states are only present in the spin down channel.

occ	$E_G^{\text{up, eigen}}$ (meV)	$E_G^{\text{dw, eigen}}$ (meV)	$E_G^{\text{tot, eigen}}$ (meV)
0.5	339	0	0
0.05	339	21.0	21.0
0.01	339	49.6	49.6
0.001	339	73.3	73.3
<0.0001	339	85.7	85.7

Table 7.3: Band gap of SQS D as a function of occupancy in the eigenvalues.

By including a threshold value to the occupancy and calculate the eigenvalue band gap at certain thresholds we find that the band gap increase as we neglect more defect states. Thus we may conclude that the band gap of SQS D or lack there of is attributed to to the defects. Comparing to the density of states band gap plotted in figure 7.1, it's apparent that $E_{\text{G}}^{\text{dos}}$ correspond to $E_{\text{G}}^{\text{eigen}}(0.5, 0.5)$, thus the density of states show the band gap with all defect states present.

7.2 Local and projected density of states

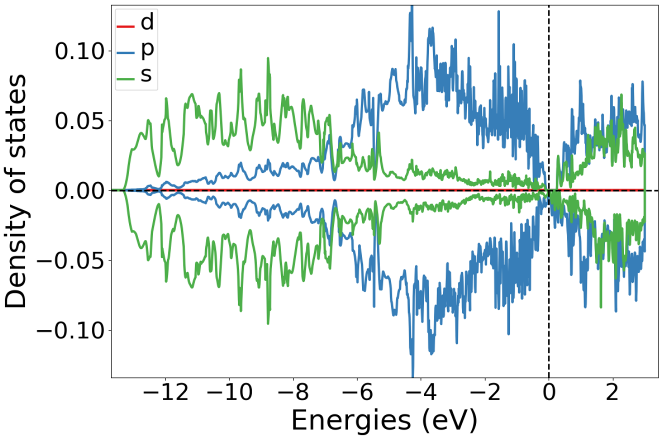

Figure 7.3: Local density of states of Si (SQS D)

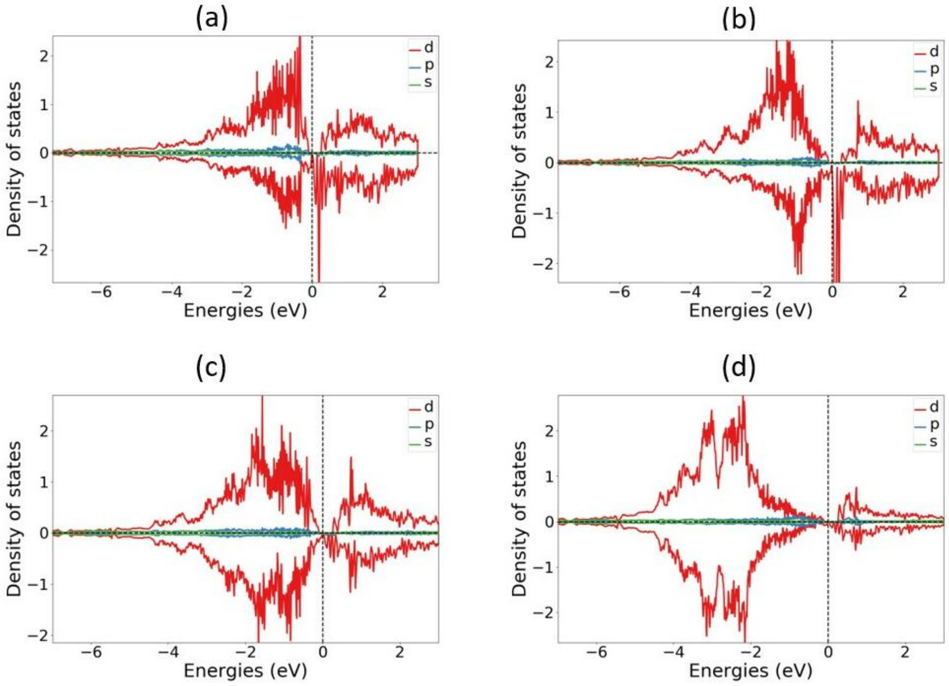

Figure 7.4: Local density of states of (a) Cr, (b) Mn, (c) Fe, (d) Ni in SQS D.

In the local density of states plotted in figure 7.3 we see that the s-electrons in Si occupy states in the lower energy regions and p electrons at slightly elevated energies closer to the Fermi energy, above E_F states are occupied by both s and p electrons almost equally. Further, the local density of states of the transition metals chromium, manganese, iron and nickel in SQS D is displayed bellow in figure 7.4. In spin down, manganese is most dominant especially above E_F, but also bellow E_F. Likewise chromium show a strong presence above the Fermi energy in spin down. Both iron an Nicel show largest contribution at energies further from the Fermi energy, most notably bellow E_F. In the spin up channel we see a similar trend where chromium lie closest to E_F followed by manganese then iron and lastly nickel at the lowest energies. Another interesting observation is that the the LDOS of iron and nickel is much more symmetric between spins, than Cr and Mn. Comparing to the LDOS of iron and silicon in bulk $\beta-$ FeSi$_2$ [5] we find good agreement for both Fe and Si in this alloy .

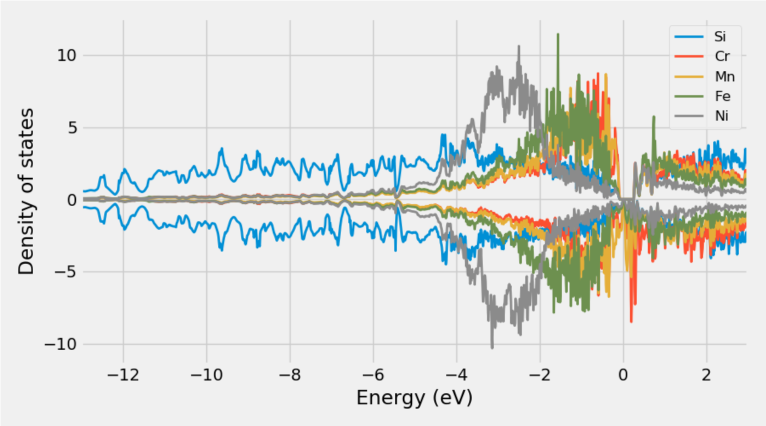

Figure 7.5: Projected density of states SQS D CFMN (fesi2) from PBE calculation

Moreover the relative positions and interplay between 3d elements and silicon as shown in the projected density of states (figure 7.5) is in good agreement with observed trends in simpler Si-rich transition metal silicides [6]. The electronic structure tends to be dominated by TM d electrons, and the valence band density of states are filled by non-bonding d states near E_F. The p-d hybridization between Si and TM elements typically fall about 6 eV bellow E_F and Si *s* states about 10 eV bellow. In our case we find that the Si states are pushed up closer to the fermi energy by random alloying of various 3d elements.

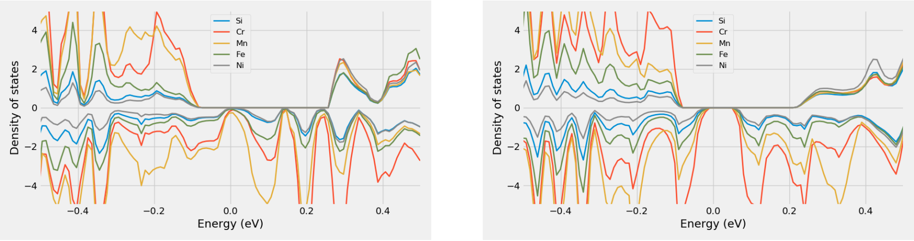

(a) SQS D

(b) SQS B

Figure 7.6: Projected density of states of SQS D and B around E_F

Above we have included the PDOS of SQS D and B but focused around E_F, from these figures we find that the spin down channel in D contain a more dominant presence of manganese especially, and some chromium as compared to the semiconducting SQS B.

7.3 Results from SCAN and HSE06 functionals

As expressed previously in this work we invoke 3 level of depths GGA (PBE), meta-GGA (SCAN) and hybrid functional (HSE06) to determine the band gap of the SQSs, these results are showcased in table 7.4. Note that we do not specify eigen/dos or the occupancy here, because par SQS D the eigenvalues does not contain defect states, hence $E_{\mathrm{G}}^{\mathrm{eigen}}(0.5) = E_{\mathrm{G}}^{\mathrm{dos}}$.

SQS	XC-functional	E_G^{up} (eV)	E_G^{dw} (eV)	E_G^{tot} (eV)
A	PBE	0.0815	0.0521	0.0281
	SCAN	0	0	0
	HSE06	0.7084	0.0261	0.0261
B	PBE	0.2932	0.0523	0.0523
	SCAN	0.1470	0.0890	0.0890
	HSE06	0.2855	0.1819	0.1819
C	PBE	0.2355	0.0343	0.0343
	SCAN	0.0690	0.1124	0.1124
	HSE06	0.1744	0.0328	0.0196
D	PBE	0.3386	0	0
	SCAN	0	0.1086	0
	HSE06	0.3780	0	0
E	PBE	0.3078	0.0495	0.0495
	SCAN	0.1540	0.1112	0.1048
	HSE06	0.5476	0.0133	0.0133

Table 7.4: Band gap calculated with PBE, SCAN and HSE06 XC-functionals of (CrFeMnNi)Si_2 SQSs.

We will begin dissecting table 7.4 by comparing SCAN to PBE. The first distinction we make notice of is in SQS A. In this supercell calculations with the SCAN functional predicts a metalic compound, contrary to the the PBE band gap of 0.03 eV. Alike the band gap of SQS D discussed previously, the 0 band gap in this structure with SCAN is caused by defect states. Neglecting such states and evaluating the band gap from just completely filled and empty eigenstates yield $E_{\mathrm{G,\,SCAN}}^{up,eigen}(0.99, 0.01) = 0.0316$ eV and $E_{\mathrm{G,\,SCAN}}^{dw,eigen}(0.99, 0.01) = 0.0531$ eV, and a resulting semiconductor with a band gao of 0.0316 eV. This value seems to agree better with the PBE band gap of this supercell, but we observe that E_G^{up} is larger in PBE. This is a recurrent patter with SCAN across all five SQSs, where $E_{\mathrm{G,\,SCAN}}^{\mathrm{up}} < E_{\mathrm{G,\,PBE}}^{\mathrm{up}}$, and moreover $E_{\mathrm{G,\,SCAN}}^{\mathrm{dw}} > E_{\mathrm{G,\,PBE}}^{\mathrm{dw}}$. This can be seen in figure 7.7, where we plot the density of states of SQS E (a, b) and C (c, d). Note that the SCAN band gap in C have the opposite spin polarization compared to PBE, this is also the case in SQS D.

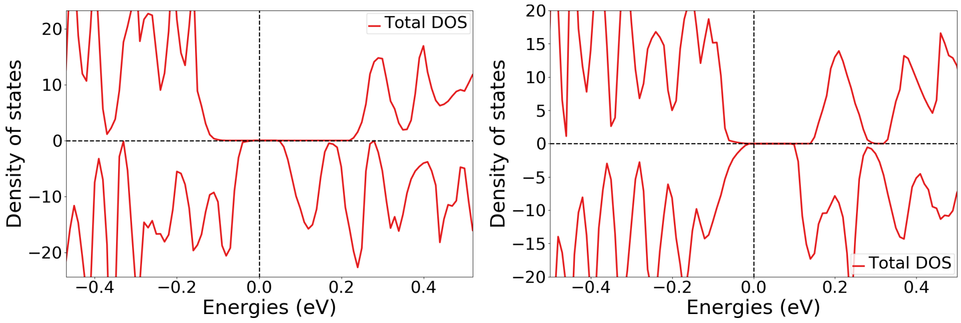

(a) SQS E PBE

(b) SQS E SCAN

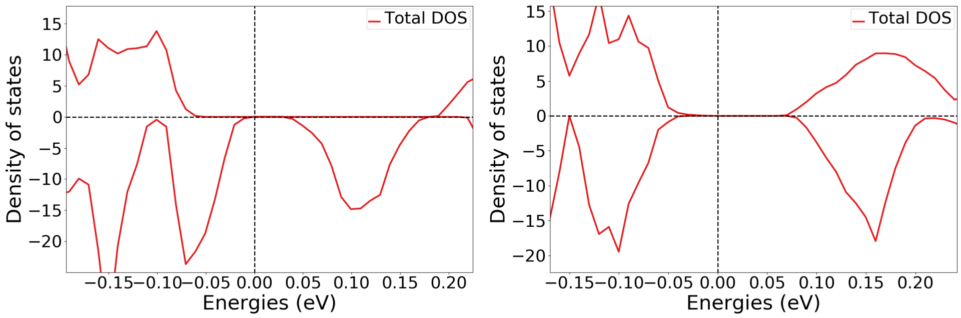

(c) SQS C PBE

(d) SQS C SCAN

Figure 7.7: Density of states illustrating the band gaps from PBE and SCAN calculations for SQS E and D.

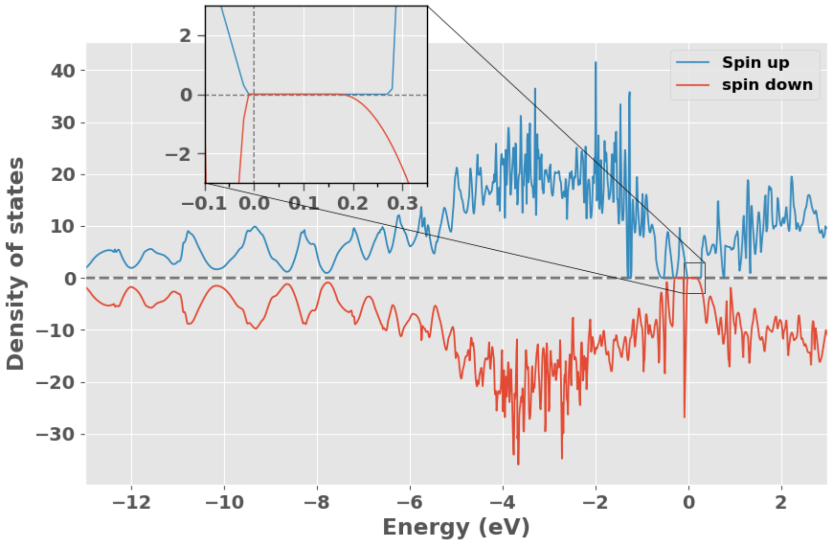

Figure 7.8: Density of states of SQS B with HSE06

With the HSE06 functional we observe the opposite trend in SQS A and E, where $E^{\mathrm{up}}_{\mathrm{G,\,HSE06}} > E^{\mathrm{up}}_{\mathrm{G,\,PBE}}$ and $E^{\mathrm{dw}}_{\mathrm{G,\,HSE06}} < E^{\mathrm{dw}}_{\mathrm{G,\,PBE}}$. But in other cases

$E^{\mathrm{up}}_{\mathrm{G,\,HSE06}}$ is lesser (SQS C) or similar to PBE (SQS B and D). On the other hand $E^{\mathrm{dw}}_{\mathrm{G,\,HSE06}}$ is consistently smaller in all structures compared to PBE, with the exception of SQS B. In this structure the HSE06 functional predicts large band gaps in both spins, as seen from the density of states plotted in figure 7.8.

As we covered in section 5.1, the hybrid functional is much more computationally demanding compared to SCAN and PBE. To reduce the cost of the HSE06 functional we performed such calculations in this project with a lower density of k-points, see section 6.1. The narrow mesh of k-points is an important factor to mention in relation to the HSE06 band gaps, that could lead to artificially exaggerated band gaps as the low density of k-points could fail to encapsulate the exact minimum transition between the valence band and conduction band.

XC-functional	Transition (k-point)
PBE	(0.250,0.000,0.250) → (0.000,0.000,0.000)
SCAN	(0.250,0.000,0.250) → (0.000,0.333,0.000)
HSE06	(0.500,0.000,0.000) → (0.000,0.000,0.000)

Table 7.5: Minimum gap between k-point in valence band and conduction band in SQS B from PBE, SCAN and HSE06

From table 7.5, we observe that all 3 functionals find different band gaps, a concerning factor is that the highest energy k-point in the valence band from PBE calculations (0.250, 0.000, 0.250) is not considered in the HSE06 calculation with the narrow grid of 2x2x2 k-points. Thus one may suspect that the HSE06 calculation overlook the minimum transition and hence return an enlarged band gap. This could for instance be the case in $E^{up}_{\mathrm{G,\,A}}$ and $E^{dw}_{\mathrm{G,\,B}}$ where HSE06 predicts much larger values compared to PBE. However without an experimental baseline of the structure, we can not conclude that this is the case. As in the other SQSs we find examples where HSE06 produce similar or lower values than PBE despite of the smaller number of k-points. The concept of sufficient k-points is especially an important matter in metallic systems, as these are known to require a more dense mesh of points to accurately map the Fermi-surface [7]. However, further investigation of the importance of k-points was not possible within the time-frame of this project.

As stated in section 6.2, we did not manage to converge hybrid calculations with the tetrahedron method, and overcame this problem by first calculating the charge density with Gaussian smearing and utilize the density to expedite calculation with TBC. The respective band gaps from these methods are displayed in table 7.6 for the five SQSs of the (CrFeMnNi)Si_2 system. Here we calculate the band gap from the eigenvalues at different cutoff occupancy *occ* to highlight the part of defect states. Calculations with Gaussian smearing was tested with smearing width *sigma* equal to 0.05 eV and 0.005 eV.

SQS	Smearing (type) width (eV)	$E_{\mathrm{G}}^{up,eigen}(0.5)$ (eV)	$E_{\mathrm{G}}^{dw,eigen}(0.5)$ (eV)	$E_{\mathrm{G}}^{up,eigen}(0.99)$ (eV)	$E_{\mathrm{G}}^{dw,eigen}(0.01)$ (eV)	$E_{\mathrm{G}}^{tot,eigen}(0.5)$ (eV)	$E_{\mathrm{G}}^{tot,eigen}(0.99, 0.01)$ (eV)
A	Gaussian (0.05)	0.7837	0.1493	-	0.2984	0.1493	0.2984
	Gaussian (0.005)	0.2117	0.1013	-	-	0.1013	-
	TBC	0.7084	0.0261	-	-	0.0261	-
B	Gaussian (0.05)	0.2783	0.1702	0.2988	0.3136	0.1506	0.2979
	Gaussian (0.005)	0.2838	0.1823	-	-	0.1801	-
	TBC	0.2855	0.1819	-	-	0.1807	-
C	Gaussian (0.05)	0.1078	0.1066	0.2405	0.1839	0.0650	0.1839
	Gaussian (0.005)	0.1304	0.0222	-	-	0.0222	-
	TBC	0.1744	0.0328	-	-	0.0196	-
D	Gaussian (0.05)	0.3661	0.0592	-	0.1872	0.0592	0.1872
	Gaussian (0.005)	ND	ND	ND	ND	ND	ND
	TBC	0.3780	0	-	0.2665	0	0.2637
E	Gaussian (0.05)	0.6653	0.1439	-	0.1675	0.1439	0.1675
	Gaussian (0.005)	0.5825	0.1211	-	-	0.1211	-
	TBC	0.5476	0.0133	-	-	0.0133	-

Table 7.6: Band gap from HSE06 calculations with gaussian smearing and smearing width *sigma* equal to 0.05 and 0.005, and the tetrahedron method (TBC). "-" mean unchanged values, "ND" means not done.

From table 7.6 we observe that the case of defect states is only a concern at larger smearing widths with Gaussian smearing. Contrary to previous cases, we find here finite band gaps despite of defect states. By comparing E_G^{up} and E_G^{dw} at $occ = 0.5$ and $occ = 0.01$, the defects appear to have a lesser role in spin up, as par SQS C the band gap in spin up is either consistent or only marginally different between the defect band gap and the hypothetical defect less band gap. E_G^{dw} on the other hand increase significantly by removing the defect states. The Gaussian smearing method is generally in better agreement with TBC at lower smearing width. But even in this case we find several dissimilarities. In A and E E_G^{dw} is larger with the Gaussian method, additionally E_G^{up} is much lower in A. In this project we have based our choice of numerical smearing on the advice on the VASP manual that state that for accurate total energies and density of states in semiconductors one should opt for the tetrahedron method [8]. However since our system is comprised of metals we include the results from utilizing Gaussian smearing as well. There are of course many more factors that affect the accuracy and reliability of both methods, but these are outside the scope of this project.

As a conclusion on the discussion of exchange-correlation functionals and the band gap of the (CrFeMnNi)Si_2 high-entropy silicide, the fact that all 3 functionals and five SQS in majority agree on the presence of a band gap is in itself an overwhelmingly positive result that allow us to state with high certainty that this hypothetical materials is in fact a semiconductor, or possibly a half-metal based on the results of the utmost stable SQS D. An additional point to this is that as covered in great detail in literature on first principles studies, the PBE functional underestimate the value of a band gap. For example in this project we determine the band gap of bulk $\beta-$ $FeSi_2$with PBE calculations to around 0.65 eV compared to the experimental value of 0.85 eV. For this reason any values of the band gap with PBE would with high probability be replicated/increased in the real material. Compared to the nonmagnetic bulk material we find these alloys to yield sensible results, here we create a random alloy that as known will introduce defect states and hence lower the band gap and further make the material magnetic. We observe that this is most apparent in spin down as the the spin up gap is more comparable to the values of the parent $FeSi_2$ structure. In the next section we will look at the probability distribution functions before considering factors related to the special quasi-random methods in section 7.5.

Compare PBE, SCAN, HSE06, SCAN opposite polarization compared to PBE and HSE06.

Compare PBE, SCAN and HSE06 bulk $\beta-$ $FeSi_2$ and computation time

Add figure CPU time.

7.4 Pair distribution functions

The probability distribution functions of SQS D and E can be seen bellow in figure 7.10, the PDFs corresponding to the remaining SQSs can be found in appendix .. . We include the PDFs of SQS D and B because as stated D is the most stable atomic configuration and hence the most representative of a potential real compound, and B to investigate distinctions between the half-metallic structure D and the semiconducting B which with HSE06 yielded substantial band gaps in both spins, recalling also that this is just very slightly bellow D in terms of stability. In the analysis we will put special emphasis on the nearest neighbor interactions since these are the most crucial in deciding the functional properties of a material.

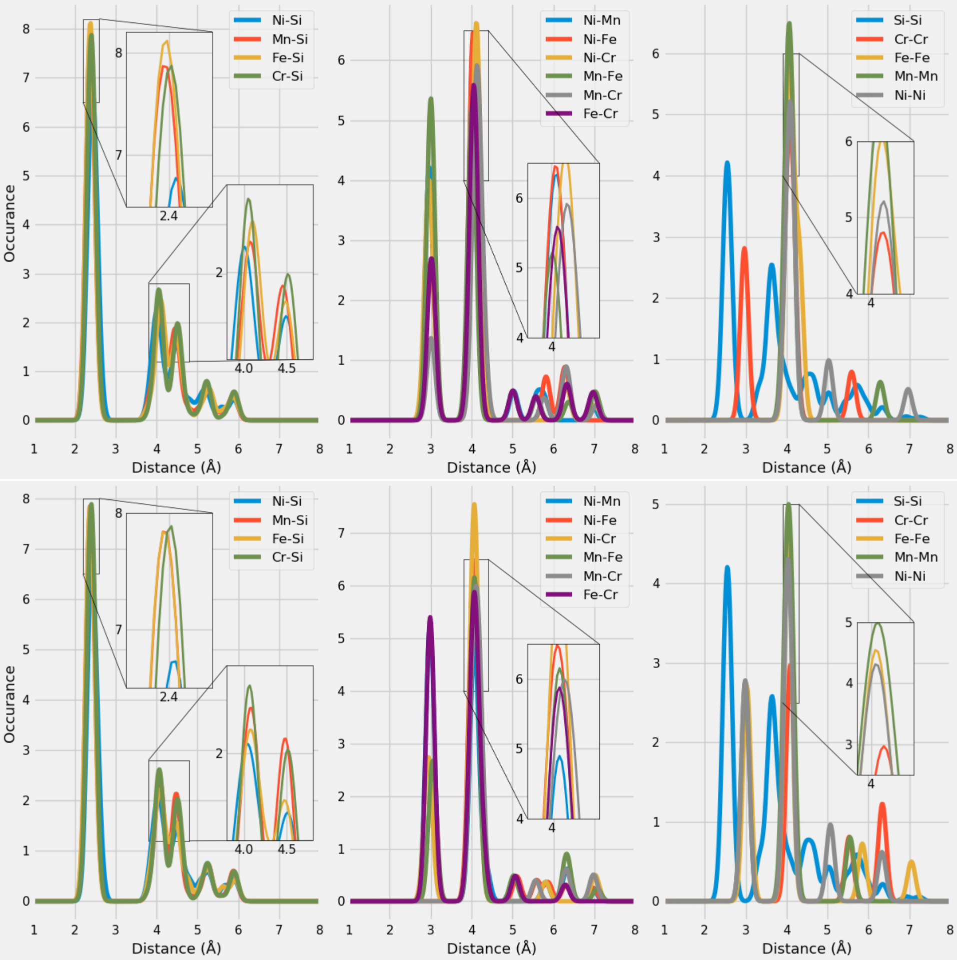

Figure 7.9: Probability distribution function of SQS D (top) and B (bottom)

We see that the relative positions of the PDFs remain consistent though both SQSs. With the aid of the ICSD (insert citation), we can compare the figure .. to the expected PDFs based on a number of experiments from a host of different compounds. As our compound contain a total of 15 different bonds, comparing each one to the ICSD values would be an exhaustive process. For our purpose we are satisfied by comparing the 4 different metal-Si bonds. We find that the preferred bond-length of TM-Si is observed at two values, the most dominant being the shorter of the two. For Fe-Si these are between 2.25-2.75 and 4-5, Mn-Si 2.25-2.75 and 3.5-5. Ni-Si lie between 2.25-2.5 and 3.85-5 and Cr-Si between 2.35-2.65 and 4-5.Clearly, the PDFs of the alloys are in good agreement with the listed values for Tm-Si bonds, with the most occurring bond length falling at around 2.4 Å for all TMs, and lesser occurrence between 4.0 - 4.5 Å. The height of the respective peaks is somewhat consistent in both structures, other than slightly reduced Fe-Si occurrence at 2.4 Å in B.

In contrast to the TM-Si bonds, we observe several distinctions between metal bonds in SQS D and B. Covering all would be tedious and not to insightful, instead we emphasize the bonds of Mn and Cr as this is where we found the biggest discrepancy in the PDOS. From the different TM-TM bonds (middle) of figure 8.8 we observe that the Mn-Fe bonds are most occurring at short distances in D and bigger distances in B, meaning that manganese and iron atoms are placed further from each other in structure D. **correct?** Similarly the bonds between Cr and Fe indicate that these atoms lie closer in B than D. In contrast the nickel and manganese/chromium bonds point to a closer distance in B for Ni-Mn and Ni-Cr in D, and a greater distance between Ni and Mn in D and Ni and Cr in B. **Litt kronglete kanskje?** In terms of the homogeneous bonds, the properties of both Cr-Cr bonds and Mn-Mn bonds are more or less alike in both structures besides some majority at shorter distance in D (The red Cr-Cr line at 3Å is underneath the grey Ni-Ni line in B in figure 8.8 (bottom right)). A more significant distinction is that both Ni-Ni and Fe-Fe bonds are found at 3 Å and 4 Å in B, but exclusively 4 Å in D.

Both the Fe-Fe and Ni-Ni bonds are in better agreement with the ICSD histograms, as the most occurring distance for these bonds are between 4-4.9 Å and additionally around 2.5 Å. **More comparisons to ICSD, ask O.M**. As a conclusion on the PDFs of this compound, we locate a pattern where the Si-Si bonds are identical and only very minor differences between TM-Si bonds in SQS D and B. This is a result of how the structures are generated with the SQS method. In th FeSi2 structure the silicon atoms are placed as before in the new supercells, but the TM elements are "randomly" distributed. Thus, it's reasonable that also here we would find the major differences between SQSs in the PDFs.

7.5 SQS size

Above we have presented the results of a high-entropy silicide (CrFeMnNi)Si_2 investigated by 5 48 atom SQSs with a volume of 700Å^3. This intermediate size allowed for the use of more complex XC-functionals, and secondly enabled a broad study of distinct permutations and compositions as we will discover in the next chapters. However the application of the special quasi-random structures method to HEAs is not necessarily straightforward. Recalling from section 4.3 the first initial concern is the size of the SQS model and if it's sufficient enough to correctly model the disordered multi-component structure. In this section we will consider this problem by studying the difference between the 48 atom SQS to that of a 96 and 192 atom SQS with volume 1200Å^3 and 2400 Å^3 respectively. In figure 7.11 we plot the reported CPU time in hours between the 3 SQS sizes, which follows roughly a N^3 dependence.

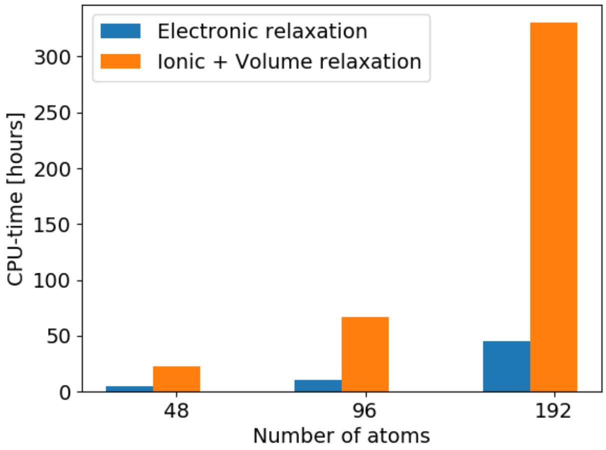

Figure 7.10: CPU time, **Make log plot instead**

Bellow we list the mean and standard deviation of the total energy, magnetic moment and enthalpy of formation of the 3 sizes in table 7.6, and band gaps in table 7.7.

SQS size	Toten (eV)		Mag (μ_B)		ΔH (eV)
	mean	std	mean	std	mean
48 atoms	- 6.6105	..	0.0833	0.0000	-11.5000
96 atoms	- 6.6092	0.0021	0.0708	0.0114	- 22.8752
192 atoms	- 6.6123	0.0022	0.0761	0.0171	- 46.6654

Table 7.7: Overivew 48, 96 and 192 SQSs.

As seen from table 7.4 both the total energy and magnetism remain more or less consistent throughout all sizes, this is a good indication of that the 48 atom model can adequately model the alloy. **Something on the formation enthalpy.** The band gap as seen in table 7.7 is first of all evident across all 3 SQS models and show similar polarization favoring the spin up direction. In several cases, we find that the magnitude of the band gap lessen with increasing SQS size.

SQS size	SQS	$E_{\mathrm{G}}^{up,eigen}(0.5)$ (eV)	$E_{\mathrm{G}}^{dw,eigen}(0.5)$ (eV)	$E_{\mathrm{G}}^{tot,eigen}(0.5)$ (eV)
48 atoms	A	0.0815	0.0521	0.0281
	B	0.2932	0.0523	0.0523
	C	0.2355	0.0343	0.0343
	D	0.3386	0	0
	E	0.3078	0.0495	0.0495
96 atoms	**A**	0.1705	0.0442	0.0367
	B	0.1386	0.0270	0.0270
	C	0.1347	0.0363	0.0075
	D	0.0892	0.0398	0.0398
	E	0.1610	0	0
192 atoms	A	0.1197	0.0321	0.0321
	B	0.1444	0	0
	C	0.1867	0	0
	D	*0.0478*	*0.0339*	0
	E	*0.0131*	*0.0184*	*0.0131*

Table 7.8: Band gap of SQSs of 48, 96 and 192 atoms each of (CrFeMnNi)Si_2. The names are arbitrary, ie A in 48 does not equal A in 96 or 192.

Similar to structure D in the 48 atom SQS we find that the 0 value in SQS E in the 48 atom model suffers from defect states and find $E_{\mathrm{G}}^{dw,eigen}(0.90, 0.10) = 0.016$ eV. The same is true for SQS B and C (192), but require $occ = 0.999, 0.001$ to locate a small nonzero spin down band gap. The band gap in SQS D and E (192) on the other hand is finite at $occ = 0.5$ but can be enlarged from increasing occ. In D we get $E_{\mathrm{G}}^{up,eigen}(0.99) = 0.075$ eV and $E_{\mathrm{G}}^{dw,eigen}(0.01) = 0.05$ eV and similarly $E_{\mathrm{G}}^{up,eigen}(0.99) = 0.05$ eV, and $E_{\mathrm{G}}^{dw,eigen}(0.01) = 0.048$ eV in E. In such cases where the eigenvalues inclusive of defect states return a finite band gap, the density of states does not. This is seen in figure .. for SQS E (192).

Drawing any conclusion on the band gaps is difficult seeing as we find very different results within the all 3 sizes. Based solely on the most stable SQS it's clear that the larger cell produce a much lower and different band gaps compared to the moderate SQS sizes which are much more similar. However also here we find that the gap in the 96 cell is only abort half of the 48 atom cell. However as seen in table 7.7 we also find evidence of large band gaps in the larger cells in other atomic configurations. This goes back

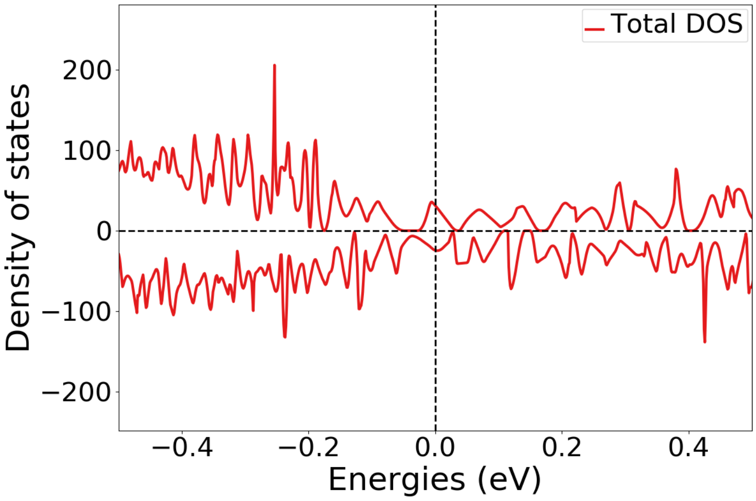

Figure 7.11: Density of states of SQS E 192 atom SQS.

to section .. when we mentioned that one of the biggest drawbacks of the special quasi-random structures method is the large number of possible atomic configurations, thus in order to conclude between results in this project the most sensible point is to consider the most stable SQS, but as seen from the very varying properties between SQSs of the same model, this does not necaccarly been the most stable SQS if we trialed 20 SQSs instead of just 5. An additional point is the magnetic property, here we only applied one configuration to base the stabiliy on, thus it's very probable that fine tuning the magnetic moments could result in different properties.

Looking at the pair distribution functions in figure 7.11 we see that the local ordering and short-range interactions is well represented and identical across all three sizes. The distinctions of preferences could as stated above simply be a product of the uniqueness of the SQSs more so than the size. On the other hand the larger SQSs clearly provide a better description of large-range interactions, that is not nearly as present in the smaller cell. However as seen in table 7.4 and in accordance with the fundamental concept of the special quasi-random structures method is that the functional properties is mostly determined by short-range effects in the lattice. Therefore, even though the bigger SQSs is a more accurate model the improvement is not justified from the cost, as illustrated in figure 7.12. And the apparent larger concern from appling the SQS method in this project is the uniqueness of each SQS.

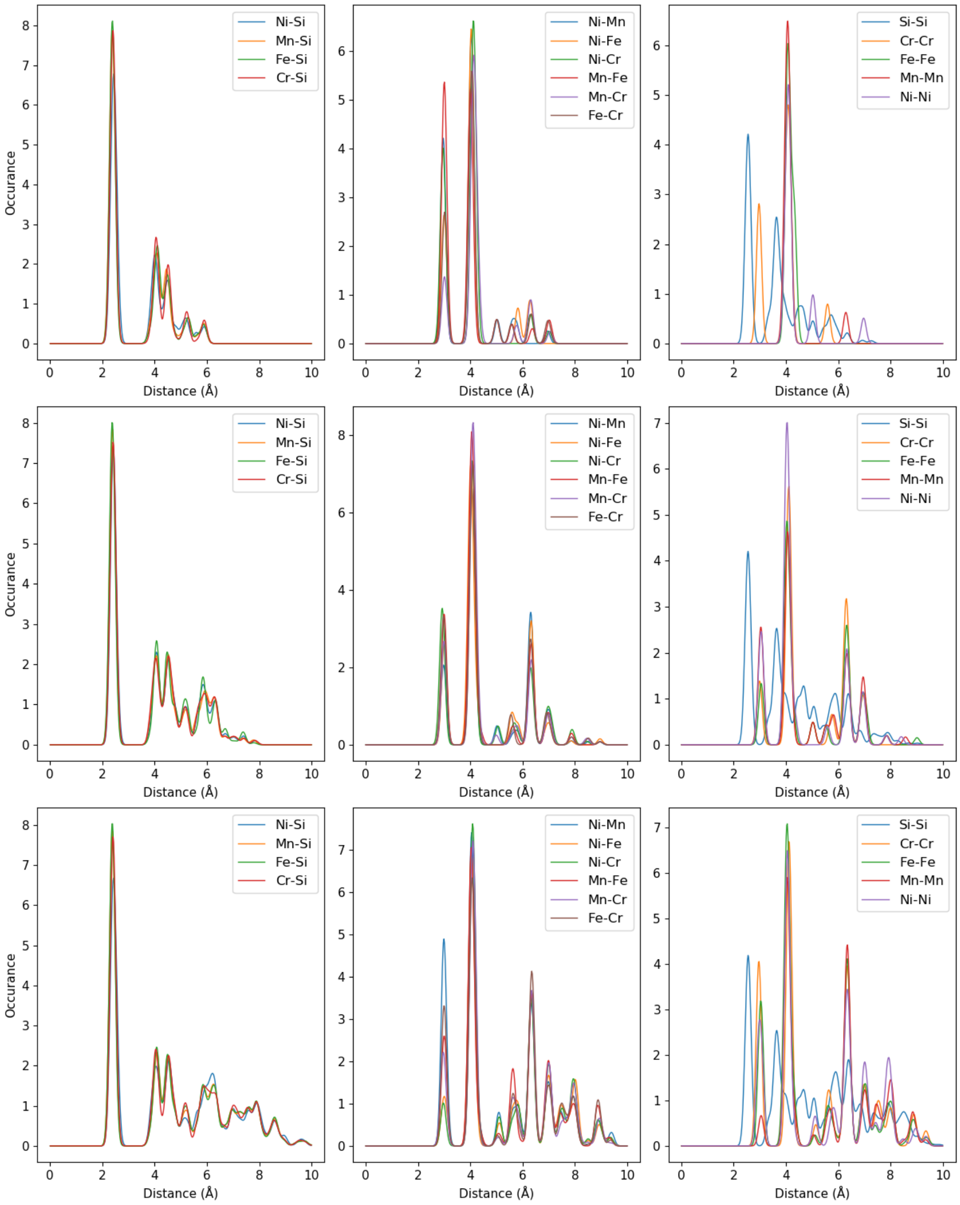

Figure 7.12: Pair distribution functions of SQS sizes (top) 48 atoms, (middle) 96 atoms, (bottom) 192 atoms

Part IV

Conclusion

Write conclusion here

Bibliography

[1] S. J. Clark et al. 'Structure and electronic properties of $FeSi_2$'. In: *Phys. Rev. B* 58 (16 Oct. 1998), pp. 10389–10393. DOI: 10.1103/PhysRevB.58.10389. URL: https://link.aps.org/doi/10.1103/PhysRevB.58.10389.

[2] Tingting Zuo et al. 'Tailoring magnetic behavior of CoFeMnNiX (X = Al, Cr, Ga, and Sn) high entropy alloys by metal doping'. In: *Acta Materialia* 130 (2017), pp. 10–18. ISSN: 1359-6454. DOI: https://doi.org/10.1016/j.actamat.2017.03.013. URL: https://www.sciencedirect.com/science/article/pii/S1359645417302008.

[3] Old řich Schneeweiss et al. 'Magnetic properties of the CrMnFeCoNi high-entropy alloy'. In: *Phys. Rev. B* 96 (1 July 2017), p. 014437. DOI: 10.1103/PhysRevB.96.014437. URL: https://link.aps.org/doi/10.1103/PhysRevB.96.014437.

[4] Voicu Popescu and Alex Zunger. 'Effective Band Structure of Random Alloys'. In: *Phys. Rev. Lett.* 104 (23 June 2010), p. 236403. DOI: 10.1103/PhysRevLett.104.236403. URL: https://link.aps.org/doi/10.1103/PhysRevLett.104.236403.

[5] R. Eppenga. 'Ab initio band-structure calculation of the semiconductor β-FeSi2'. In: *Journal of Applied Physics* 68.6 (1990), pp. 3027–3029. DOI: 10.1063/1.346415. eprint: https://doi.org/10.1063/1.346415. URL: https://doi.org/10.1063/1.346415.

[6] H Lange. 'Electronic properties of semiconducting silicides'. In: *physica status solidi (b)* 201.1 (1997), pp. 3–65.

[7] Stewart Clark. 'Modelling complex structures'. URL: http://cmt.dur.ac.uk/sjc/thesis/thesis/node28.html.

[8] *ISMEAR - Vaspwiki*. URL: https://www.vasp.at/wiki/index.php/ISMEAR.